LAWRENCE
LIVERMORE
NATIONAL
LABORATORY

UCRL-JRNL-232829

Milestones in EBIT Spectroscopy and Why it Almost Didn't Work

R. E. Marrs

July 18, 2007

Canadian Journal of Physics

Milestones in EBIT Spectroscopy and Why it Almost Didn't Work

R. E. Marrs

Lawrence Livermore National Laboratory

Livermore, CA 94551

Abstract

The EBIT spectroscopy that now seems routine would not be possible without considerable good luck in several areas of EBIT technology. Among these are x-ray background, ion cooling, neutral gas density, and electron current density and energy control. A favourable outcome in these areas has enabled clean x-ray spectra, sufficient intensity for high resolution spectroscopy, production of very high charge states, and a remarkable variety of spectroscopic measurements. During construction of the first EBIT 20 years ago, it was not clear that any of this was possible.

PACS numbers: 34.80.Kw, 32.30.Rj

Keywords: EBIT; ion trap; x-ray spectroscopy; electron-ion collisions

Corresponding author

Phone: 925-422-3890

e-mail: marrs1@llnl.gov

Introduction

The contributions to this workshop and publications in the literature document the development of EBIT spectroscopy during the past 20 years, including the amazing variety and quantity of measurements. Newcomers to the field may not realize how remarkable this seems to those who remember the development of the first EBIT – at that time it was not obvious that the EBIT would work. Many things could have gone wrong, and didn't. In this paper I review how favorable outcomes in several key aspects of EBIT technology enabled different types of EBIT spectroscopy.

The EBIT was preceded by several important developments. Sequential ionization of ions confined in the space charge of an electron beam was demonstrated in 1957 if not earlier, but only relatively low charge states such as Hg^{5+} were produced at that time [1]. The most important predecessor of the EBIT was the electron beam ion source (EBIS), which by 1986 had demonstrated the production of neonlike Xe^{44+} and higher charge states, thereby demonstrating the feasibility of producing very high charge states by ion confinement in electron beams [2].

Before the construction of the first EBIT, there was one measurement of x rays from electron-ion collisions in an EBIS, performed by looking through a hole in the cathode of the electron gun [3]. The difficulty of adapting an EBIS for spectroscopy, as well as the difficulty of producing very high charge states in a room temperature apparatus was demonstrated to the EBIT developers during work with an EBIS at Lawrence Berkeley

National Laboratory and influenced the design of the EBIT [4]. This was the state of the art in 1985 – 1986 when the first EBIT was constructed at Lawrence Livermore National Laboratory.

Design of the first EBIT

Key features of the first EBIT are illustrated in Fig. 1, a widely shown drawing almost as old as the EBIT itself. The Helmholtz-coil geometry provides a uniform magnetic field (and hence uniform electron beam density) over the ion trapping region, and allows multiple radial lines of sight for spectroscopy. The roughly two-cm length of the ion trap is sufficient for spectroscopy. The ions are confined radially by the space charge potential of the electron beam and axially by a programmable low voltage (compared to the electron beam energy) barrier.

Some critical features of the EBIT may not be apparent from Fig. 1. One of these is the high electron beam current density. The x-ray emission rate from trapped ions is given by

$$Y_x = j_e \, \sigma \, N_i \qquad (1)$$

where j_e is the electron beam current density, σ is the cross section for the x-ray production process, and N_i is the number of ions in the electron beam. Since the x-ray emission rate is proportional to the electron beam current density, the EBIT was designed

to have a high current density. This was achieved by using superconducting magnet coils to produce a high (3-T) magnetic field in the trap because this field compresses the beam, and by carefully designing the magnetic field profile near the electron gun for zero magnetic field on the cathode because a cathode magnetic field inhibits beam compression.

Another important feature of the first EBIT is the operation of the trap electrodes (drift tubes) at a temperature of 4 K, the use of small holes in the end electrodes, and the use of beryllium x-ray windows at 4 K on the radial openings. This was done to minimize the neutral gas density in the trap, knowing that high ion charge states are destroyed by charge exchange recombination with neutral molecules.

The inside surface of the center trap electrode is in the field of view of spectrometers attached to the radial ports. The inside diameter of the center electrode was therefore made larger than that of the end electrodes partly out of fear that it could be a source of bremsstrahlung radiation if struck by electrons in the fringes of the main electron beam. If so, the bremsstrahlung radiation could overwhelm x-ray emission from the trapped ions.

First spectroscopy measurements

The first EBIT was initially equipped with a flat Bragg crystal spectrometer and a Si(Li) x-ray detector. Fortuitously, the 70-μm diameter of the compressed electron beam

provides an excellent "entrance slit" for a flat crystal spectrometer. The EBIT was operated for the first time without ion injection and with no axial trapping potential other than that generated from space charge by the different diameters of the drift tubes. The intent was to evaluate electron beam transmission and bremsstrahlung background. A small fraction of the electron beam and secondary electrons is lost due to imperfect transmission to the collector. Consider an electron beam of 100 mA at 10 keV. Taking Eq. 1 with typical EBIT parameters and multiplying by the energy of emitted x-rays gives a radiated x-ray power of $\sim 10^6$ keV/s from trapped ions. By comparison, the bremsstrahlung power from 10 uA (roughly the current drawn by the high voltage electrodes when the beam is on) of 10-keV electrons striking copper is $\sim 10^{12}$ keV/s.

The first x-ray spectra from the EBIT, similar to the Si(Li) spectrum shown in Fig.2, showed unexpected line radiation but no evidence of bremsstrahlung from the trap electrodes. The line radiation originated from high charge states of barium, evaporated or sputtered from the cathode of the electron gun. EBIT x-ray spectra are completely free of bremsstrahlung background. In fact, the x-ray count rate is negligible with the beam on and the trap potential inverted to expel ions.

Fortuitously, the influx of barium into the EBIT trap was sufficient to enable the first spectroscopy measurements but not large enough to disrupt subsequent measurements with other ions. The first spectroscopy measurement done with an EBIT was a measurement of electron impact excitation in neonlike Ba^{46+} [5]. The transitions measured are shown in Fig. 3, and examples of the spectra from which the excitation

cross sections were determined are shown in Fig. 2. This first EBIT measurement introduced the technique of measuring cross sections relative to radiative recombination on the same ions. Radiative recombination lines are almost always present in EBIT x-ray spectra, and the radiative recombination cross sections are well known. In the barium measurement, the intensity ratio of deexcitation and radiative recombination lines was determined from the Si(Li) x-ray spectra, and the Bragg crystal spectra were used to correct for the contribution of satellite lines from adjacent charge states. Other early results from the first EBIT can be found in Ref. [6].

Electron beam energy resolution and control

In contrast to plasma sources of x rays such as the tokamak, the electron beam in the EBIT is monoenergetic. In fact, the energy resolution of the electron beam is surprisingly good. The geometry of the EBIT with high voltage positive electrodes in an axial magnetic field is a Penning trap for electrons, and there are indications of Penning electrons oscillating through the apparatus, presumably at energies different from the beam energy. The large secondary electron emission coefficient of the copper electron beam collector suggests that secondary electrons could appear as a tail on the electron energy distribution. In some electron beam devices, microwave tubes being an example, the electron energy distribution is broadened by wave interactions. Any of these effects or others could have degraded the energy resolution of the EBIT electron beam.

Figure 4 shows the result of a careful measurement of the EBIT electron energy resolution for a single dielectronic recombination resonance. The 50-eV width can be attributed to the variation of space charge potential within the trap and ripple in the high voltage power supply. There is no evidence of a low-energy tail in the electron energy distribution. Even at much higher electron energy the energy resolution is good. The maximum energy of one of the EBITs at LLNL was increased to 200 keV (Super EBIT) with an energy resolution of approximately 100 eV [8].

The good energy resolution of the EBIT electron beam, combined with the capability to change the energy quickly, enabled the establishment of a favorable ionization balance at one electron energy followed by a measurement at a different electron energy. This allowed the study of excitation functions and resonant reactions such as dielectronic recombination with good electron and x-ray energy resolution simultaneously. At first, these measurements were done by switching the electron energy between two values. Later, a continuous sweep of the electron energy was used, usually with a pause at a high value between sweeps to maintain the desired ionization balance [9]. An example of data obtained with this powerful technique is shown in Fig. 5. This plot shows both resonant and non-resonant reactions, including direct excitation, resonant excitation, dielectronic recombination, and radiative recombination. All of these reactions can be resolved and measured separately because of the good resolution and control of the electron beam energy.

Ion injection

The injection of low charge ions from a metal vapor vacuum arc (MEVVA) source was implemented on the first EBIT as soon as it became operational [10]. For the past 20 years, the MEVVA source has enabled the study of many different elements in the LLNL EBITs, including rare earths and other elements that are difficult to inject by other means. Ions from a single MEVVA pulse are injected along the electron beam through a hole in the electron collector. They are captured by the rising axial barrier of the trap, timed to close in coincidence with the firing of the MEVVA [11]. The longitudinal and transverse phase space density of the MEVVA ions appears to be just right to slightly overfill the EBIT trap (although only a small fraction of the total ion output from the MEVVA is actually captured). This, along with the availability of so many different elements from the MEVVA, must be regarded as another piece of good luck that was not obvious before it was tried.

Ion heating and evaporative cooling

A calculation of ion heating by the electron beam implies that the production of very high charge states in an EBIT is impossible. This is because the ion heating rate scales as q^2 and ionization cross sections scale as $1/q^2$, where q is the ion charge. Hence there is some q beyond which the ions are boiled out of the electron beam before they can be further ionized. Trapped ions are heated by small angle Coulomb collisions with beam electrons. The heating power per ion is

$$H_i = \pi \frac{j_e}{e} \frac{q^2 e^4}{E_e} \frac{2m_e}{M_i} \lambda_{ie} \qquad (2)$$

where m_e is the mass of the electron, M_i is the ion mass, E_e is the electron beam energy, and λ_{ie} is the Coulomb logarithm [12].

For typical EBIT parameters and q = 50, the ion energy would reach the space charge potential at the edge of the electron beam in roughly 150 ms. Figure 6 shows the charge state evolution for tin (Z = 50) ions calculated for single step ionization using Lotz cross sections [13]. Sn^{40+} can be reached in 150 ms, but over one second is required to reach Sn^{48+}. Ion heating was a reason to doubt that an EBIT could produce high charge states. Furthermore, during the design of the EBIT there was some concern that electron-ion plasma instabilities could heat the ions at a much faster rate [4,14].

The discovery and application of evaporative ion cooling was the breakthrough that enabled the production of very high charge states. The loss of trapped ions by evaporation was recognized as an important process early in the EBIT program at LLNL [6]. The ion evaporation rate over a potential barrier of height V_{trap} is proportional to e^{-qeV_{trap}/T_i}, where T_i is the ion temperature. Notice that low charge ions are lost exponentially faster than high charge ions – this is the key to cooling. Since the ion-ion thermal equilibration time is fast compared to the evaporation rate, the evaporation of low-Z ions can be used to cool the high-q ions remaining in the trap. The active injection

of light elements to cool high charge states of heavy elements was initiated and refined early in the EBIT program at LLNL [6,15,16]. Evaporative cooling is so effective that it allowed Au^{69+} ions to remain trapped in the EBIT electron beam for 4 hours after a single injection of gold from a MEVVA source [16].

Because of the exponential dependence of the evaporative cooling rate on the ratio of ion temperature to trap potential, the axial trap potential tightly controls the ion temperature. (The ion temperature in turn determines the radial distribution of ions within the electron beam.) The cooling power and therefore the inventory of high charge ions retained in the trap is determined by a combination of the trap potential and the injection rate of low-Z cooling ions.

Several different light elements were examined for their effectiveness as coolants. Neon gas was found to be particularly convenient and effective, and a gas injector with collimating apertures and an adjustable injection rate was constructed. The cooling of highly charged bismuth ions by neon gas injection is illustrated in Fig. 7, which shows how the x-ray emission rate from highly charged bismuth ions is determined by the injection rate of cooling gas. In the limit of no cooling gas, there is no bismuth in the electron beam. In the opinion of the author, the development of ion cooling technology for the EBIT is remarkable. Had it not gone well, many of the spectroscopic measurements of the last 20 years would not have been possible.

The success of evaporative cooling and the versatility of the MEVVA injector enabled the study of almost any highly charged ion. An early example is the measurement of the $3p_{3/2} - 2s_{1/2}$ transition energy in neonlike Yb^{60+}, illustrated in Fig. 8 [17]. In this case, the EBIT measurement confirmed a suspected Z-dependent error in theoretical calculations of the transition energy. This measurement was proof of the ability of the EBIT to measure transition energies at higher atomic number than other sources, enabled by the achievement of long trapping times and x-ray intensity sufficient for high resolution Bragg crystal spectroscopy. The Yb^{60+} measurement provided an early example of another often-used technique in EBIT spectroscopy – x-ray wavelength calibration with transitions in another element, in this case, hydrogenlike Zn^{29+}. This works even for flat crystal spectroscopy because both elements are at the same location (the center of the electron beam).

Charge exchange recombination

The charge exchange recombination cross section for highly charged ions and neutral atoms is enormous. For example, $\sigma^{cx} \sim 2 \times 10^{-14}$ cm^2 for q = 50+ and neutral neon [18]. Interestingly, this cross section is 10 orders of magnitude larger than the electron impact ionization cross section for the most highly charged ions. The ion destruction rate by charge exchange is

$$\frac{dN_i}{dt} = n_0 v_i \sigma^{cx} \qquad (3)$$

where n_0 is the neutral gas density and v_i is the ion velocity. The neutral gas density must be low (~10^{-12} Torr equivalent pressure or less) to avoid destruction of high charge states in an EBIT. As mentioned above, several features of the EBIT design were chosen to minimize the neutral gas density in the trap. Some people thought that the desorption of gas during EBIT operation would prevent the production of very high charge states.

Ironically, after all the measures that were taken to avoid neutral gas in the EBIT trap, it is introduced intentionally for ion cooling. This does, of course, adversely affect the ionization balance as illustrated in Fig. 9. In practice, count rate and ionization balance can be traded off against each other, and conditions can be optimized for specific measurements by adjusting operating parameters such as the cooling gas density, axial trap potential, and electron beam current (and density). As suggested by Fig. 9, we are lucky that the charge exchange recombination cross sections are not larger. If they were, several milestones in EBIT spectroscopy would not have been possible.

Production of bare U^{92+}

The production of bare U^{92+} at LLNL required maximum good luck in every respect [19]. Not only were the features of EBIT discussed above stretched to their limit, but the high voltage Super EBIT was also stretched to its maximum voltage and current. (The first EBIT was converted to Super EBIT by modifying the electron gun and collector to float at a high negative potential [8].) Figure 10 shows the radiative recombination x-ray spectrum obtained for highly charged uranium ions, including K-shell recombination

onto bare and hydrogenlike ions. Cooling gas flow and other parameters were optimized for production of the highest charge states as discussed above. Because the radiative recombination cross sections are much larger than the K-shell ionization cross sections, an average of only 10 ions out of approximately 5×10^4 trapped uranium ions were in the 92+ charge state.

Despite the small number of bare and hydrogenlike ions it was possible to determine the electron impact ionization cross section for hydrogenlike uranium from the steady-state ionization balance using the relationship

$$\sigma_{H\to Bare}^{ion} = \frac{N_{Bare}}{N_H}\left[\sigma_{Bare\to H}^{RR} + \left(\frac{e}{j_e}\right) n_0 \left\langle v\sigma_{Bare\to H}^{CX} \right\rangle\right] \qquad (4)$$

Here the abundance ratio N_{bare}/N_H is determined from the radiative recombination peaks in the measured spectra, the 70-b radiative recombination cross section is known, and the last term (approximately 7 b) is the effective contribution from charge exchange. The charge exchange recombination term was corrected for by running different cooling gas densities and extrapolating to zero in a manner suggested by Fig. 9.

The measurement of the electron impact ionization cross section for hydrogenlike uranium was the first direct measurement for high-Z ions, and a test of relativistic collision theory in a simple system. The same technique was later extended to other elements and adapted for the measurement of L-shell ionization cross sections [20, 21].

Future improvements

After 20 years of EBIT spectroscopy enabled by several fortuitous developments, it is reasonable to ask whether there is any more good luck to be had. The author believes that there is. One important improvement would be a large increase in count rate. Most EBIT measurements are presently count-rate limited. That is, the final uncertainty in a measured transition energy is dominated by counting statistics. Hence a 100-fold increase in x-ray intensity would provide up to a 10-fold reduction in measured uncertainty.

Looking at Eq. 1 for x-ray intensity, we see that an increase in count rate requires an increase in the electron current density or the number of trapped ions. The electron current density j_e depends on the trap magnetic field B and properties of the electron gun. For zero magnetic field at the cathode, it is given by

$$j_e = j_c \frac{eBr_c}{\sqrt{8m_e kT_c}} \qquad (5)$$

where j_c is the cathode current density, r_c is the cathode radius, m_e is the electron mass, and kT_c is the cathode temperature. It is possible to increase j_c, r_c, and B. Increasing j_c and r_c also increases the total electron current and beam space charge, allowing a larger number of trapped ions. Figure 11 indicates how an EBIT with a higher magnetic field and upgraded electron gun might provide a 100-fold increase in x-ray intensity. In this

case, both the current density and the number of trapped ions are 10-fold greater than their values in the first EBIT. At least one group is attempting to build an EBIT with these parameters [22].

Conclusions

An examination of different aspects of EBIT technology reveals how they have enabled 20 years of spectroscopy. Some aspects of EBIT technology could easily have turned out badly, but didn't. These range from the fortuitous background of barium in just the right amount for spectroscopy but not too much to disrupt other measurements, to the careful development of evaporative cooling for the production and retention of very highly charged ions.

Acknowledgements

The author would like to acknowledge the contributions of the many people who have developed EBIT spectroscopy during the past 20 years and improved the EBIT itself. Special recognition is due to M. Levine, with whom the author developed the first EBIT. Important contributions to the design of the first EBIT were made by R. Wolgast, L. Hansen, and W. Hearn. This work was performed under the auspices of the U. S. Department of Energy by Lawrence Livermore National Laboratory under Contract No. W-7405-Eng-48.

References

[1] R. H. Plumlee, Rev. Sci. Instrum. **28**, 830 (1957).

[2] E. D. Donets, Physica Scripta **T3**, 11 (1983).

[3] J. P. Briand et al., Phys. Rev. Lett. **52**, 617 (1984).

[4] M. A. Levine, R. E. Marrs, and R. W. Schmieder, Nucl. Instrum. Methods A **237**, 429 (1985).

[5] R. E. Marrs, M. A. Levine, D. A. Knapp, and J. R. Henderson, Phys. Rev. Lett. **60**, 1715 (1988).

[6] M. A. Levine, R. E. Marrs, J. R. Henderson, D. A. Knapp, and M. B. Schneider, Phys. Scr. T22, 157 (1988).

[7] P. Beiersdorfer, T. W. Phillips, K. L. Wong, R. E. Marrs, and D. A. Vogel, Phys. Rev. A **46**, 3812 (1992).

[8] D. A. Knapp, R. E. Marrs, S. R. Elliott, E. W. Magee, and R. Zasadzinski, Nucl. Instrum. Methods A **334**, 305 (1993).

[9] D. A. Knapp, R. E. Marrs, M. B. Schneider, M. H. Chen, M. A. Levine, and P. Lee, Phys. Rev. A **47**, 2039 (1993).

[10] I. G. Brown, J. E. Galvin, R. A. MacGill, and R. T. Wright, Appl. Phys. Lett. **49**, 1019 (1986).

[11] R. E. Marrs, in *Experimental Methods in the Physical Sciences Volume 29A*, edited by F. B. Dunning and R. G. Hulet, (Academic Press, San Diego, 1995), p. 391.

[12] I. P. Shkarofsky, T. W. Johnston, and M. P. Bachynski, *The Particle Kinetics of Plasmas* (Addison Wesley, Reading, MA, 1966).

[13] W. Lotz, Z. Phys. **216**, 241 (1968).

[14] C. Litwin, M. C. Vella, and A. Sessler, Nucl. Instrum. Methods **198**, 189 (1982).

[15] B. M. Penetrante, J. N. Bardsley, D. DeWitt, M. Clark, and D. Schneider, Phys. Rev. A 43, 4861 (1991).

[16] M. B. Schneider, M. A. Levine, C. L. Bennett, J. R. Henderson, D. A. Knapp, and R. E. Marrs, in *International Symposium on Electron Beam Ion Sources and Their Applications*, edited by A. Hershcovitch (Conf. Proc. No. 188, American Institute of Physics, New York, 1989), p. 158.

[17] P. Beiersdorfer, M. H. Chen, R. E. Marrs, and M. A. Levine, Phys. Rev. A **41**, 3453 (1990).

[18] R. E. Olson and A. Salop, Phys. Rev. A **14**, 579 (1976).

[19] R. E. Marrs, S. R. Elliott, and D. A. Knapp, Phys. Rev. Lett. 72, 4082 (1994).

[20] R. E. Marrs, S. R. Elliott, and J. H. Scofield, Phys. Rev. A **56**, 1338 (1997).

[21] Th. Stöhlker, A Krämer, S. R. Elliott, R. E. Marrs, and J. H. Scofield, Phys. Rev. A 56, 2819 (1997).

[22] M. Froese et al., Hyperfine Interactions (in press).

Figure Captions

Fig. 1. The electron beam ion trap.

Fig. 2. X-ray spectra from neonlike Ba^{46+} excited by 5.69-keV electrons. Top: Bragg crystal spectrum. Bottom: Si(Li) spectrum. (from Ref. [5])

Fig. 3. Transitions in neonlike Ba^{46+}. The observed x rays were used to measure excitation cross sections for the corresponding upper levels. The decay and feeding percentages are derived from theoretical rates at 5.69-keV electron energy. (from Ref. [5])

Fig. 4. Measured electron energy resolution for a single dielectronic recombination resonance. (adapted from Ref. [7])

Fig. 5. X-ray emission from heliumlike Mo^{40+} target ions obtained with a continuous sweep of the electron beam energy (drift tube voltage). The bright spots are dielectronic recombination resonances, and the diagonal bands are radiative recombination photons. (from Ref. [9].)

Fig. 6. Time required to reach different charge states of tin in a 30-keV EBIT electron beam.

Fig. 7. Dependence of the highly-charged-ion interaction rate on cooling gas density. The vertical axis is the absolute count rate of x rays from radiative recombination into the open M shell of bismuth at 192-keV electron energy. (from Ref. [20])

Fig. 8. Measurement of the 3A transition energy in neonlike Yb^{60+}. Left: Bragg crystal spectra showing (a) the Zn^{29+} Lyman-α calibration lines and (b) the measured transition in Yb^{60+}. Right: Comparison of the EBIT measurement with tokamak measurements at lower atomic number. (from Ref. [17])

Fig. 9. Trade off between ionization balance and count rate. The upper plot shows the abundance ratio of hydrogenlike and bare molybdenum ions at 65-keV electron energy. The ratio increases with increasing neutral atom density. The lower plot shows the absolute count rate for recombination into the K shell. (from Ref. [20])

Fig. 10. Production of bare and hydrogenlike uranium ions in the LLNL Super EBIT at 198-keV electron energy. The inset shows K-shell radiative recombination from a second detector. (from Ref. [19])

Fig. 11. Operating curves for different electron guns showing electron beam current density in the trap as a function cathode emission current density. The lower curve applies to the original LLNL EBIT in which the total current is limited to roughly 200 mA by voltage limitations of the electron gun. The middle curve is for a prototype gun designed and built at LLNL and tested at up to 1 A current, but never used on an EBIT –

the curve is the expected performance for a 6-T field. The upper curve is for a gun design that could provide a 100-fold increase in x-ray intensity if operated at 5 A with a 6-T trap field.

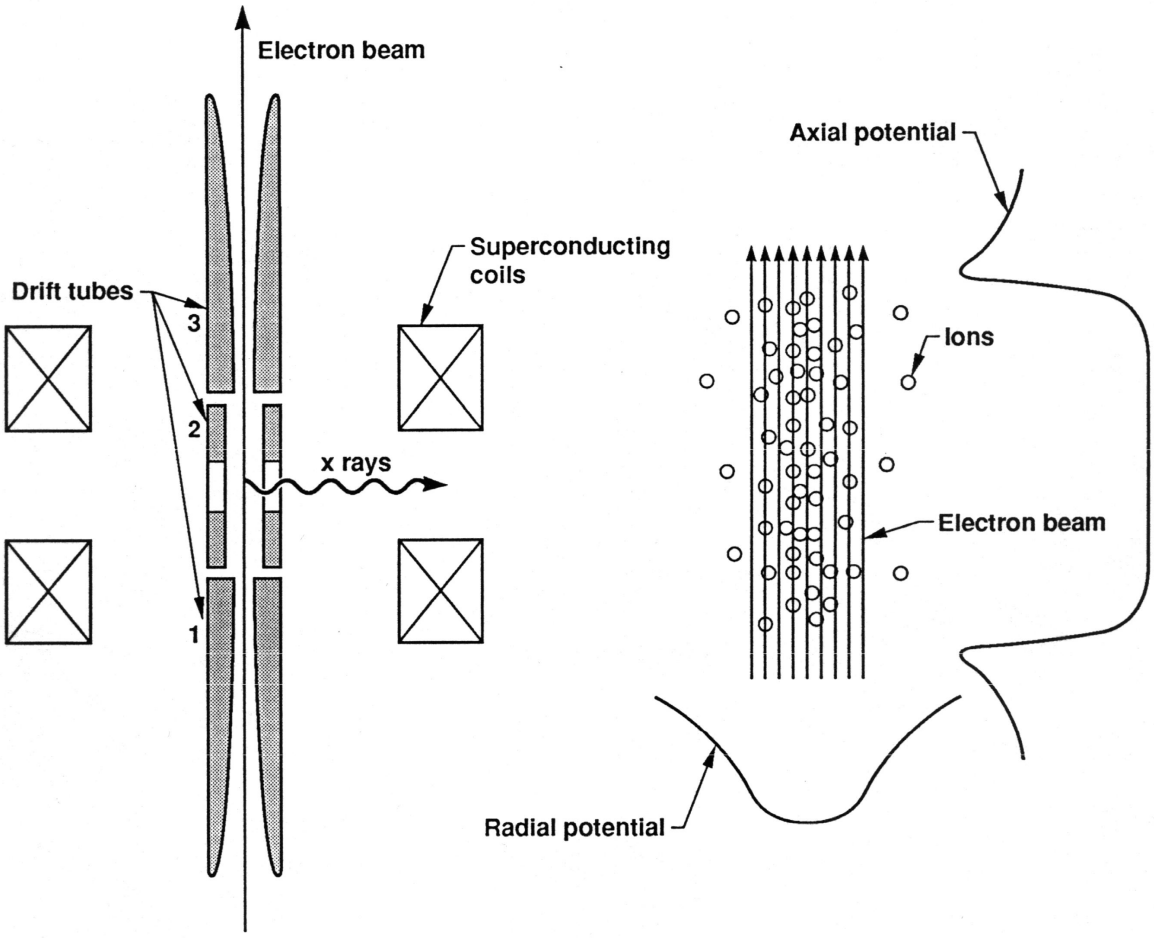
Electron beam
Drift tubes
3
2
1
Superconducting coils
x rays
Axial potential
Ions
Electron beam
Radial potential

Figure 1

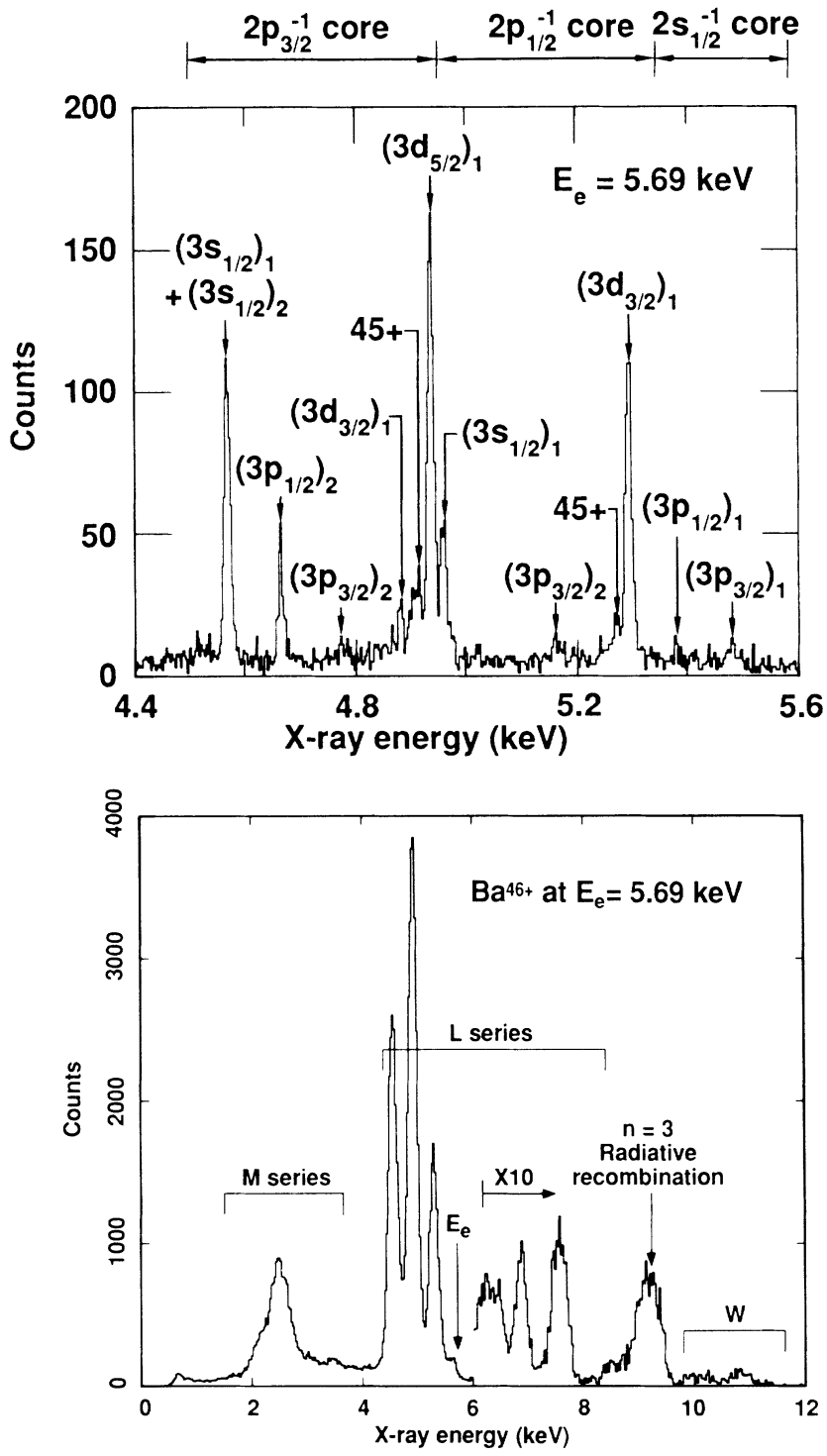
2p3/2-1 core
2p1/2-1 core
2s1/2-1 core
Counts
X-ray energy (keV)
Ee = 5.69 keV
(3d5/2)1
(3s1/2)1 + (3s1/2)2
45+
(3d3/2)1
(3p1/2)2
(3s1/2)1
(3p3/2)2
(3d3/2)1
(3p1/2)1
(3p3/2)2
(3p3/2)1
Ba46+ at Ee= 5.69 keV
L series
M series
X10
n = 3
Radiative
recombination
Ee
W

Figure 2

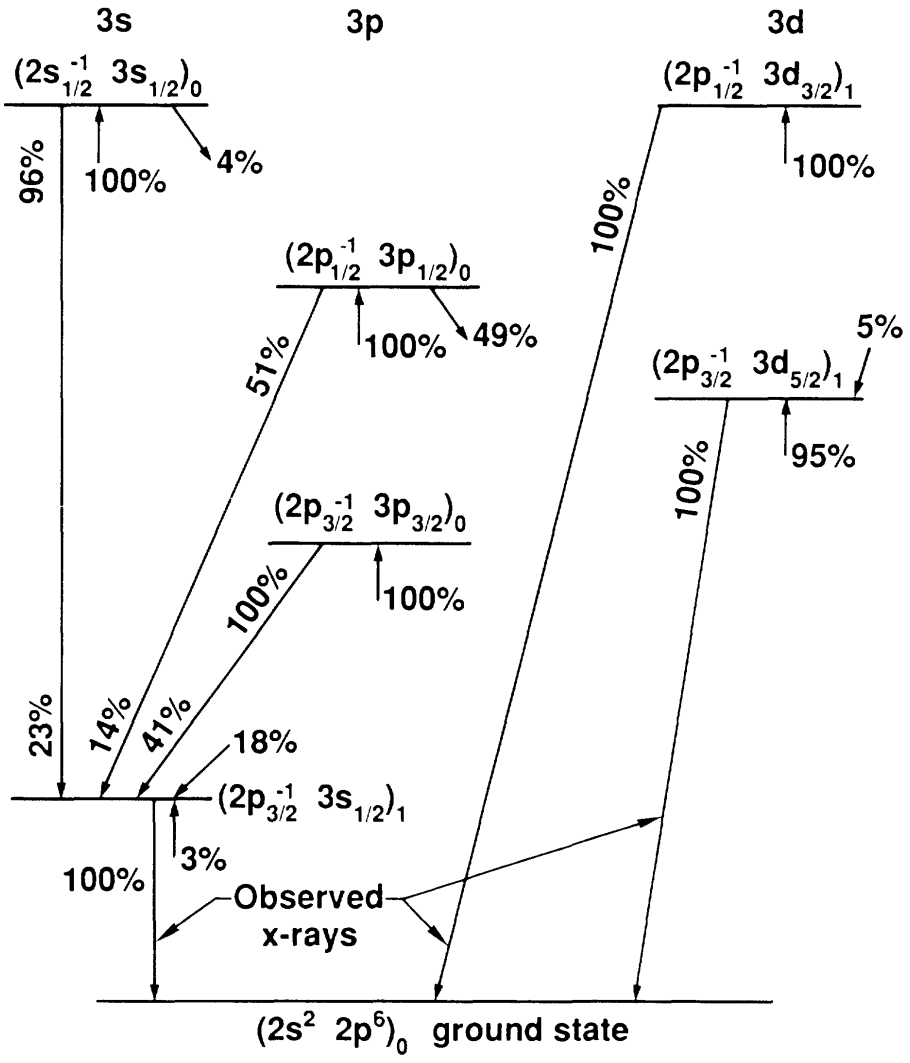
3s
3p
3d
$(2s_{1/2}^{-1}\ 3s_{1/2})_0$
$(2p_{1/2}^{-1}\ 3d_{3/2})_1$
96%
100%
4%
100%
$(2p_{1/2}^{-1}\ 3p_{1/2})_0$
51%
100%
49%
5%
$(2p_{3/2}^{-1}\ 3d_{5/2})_1$
95%
100%
$(2p_{3/2}^{-1}\ 3p_{3/2})_0$
100%
100%
23%
14%
41%
18%
$(2p_{3/2}^{-1}\ 3s_{1/2})_1$
3%
100%
Observed
x-rays
$(2s^2\ 2p^6)_0$ ground state

Figure 3

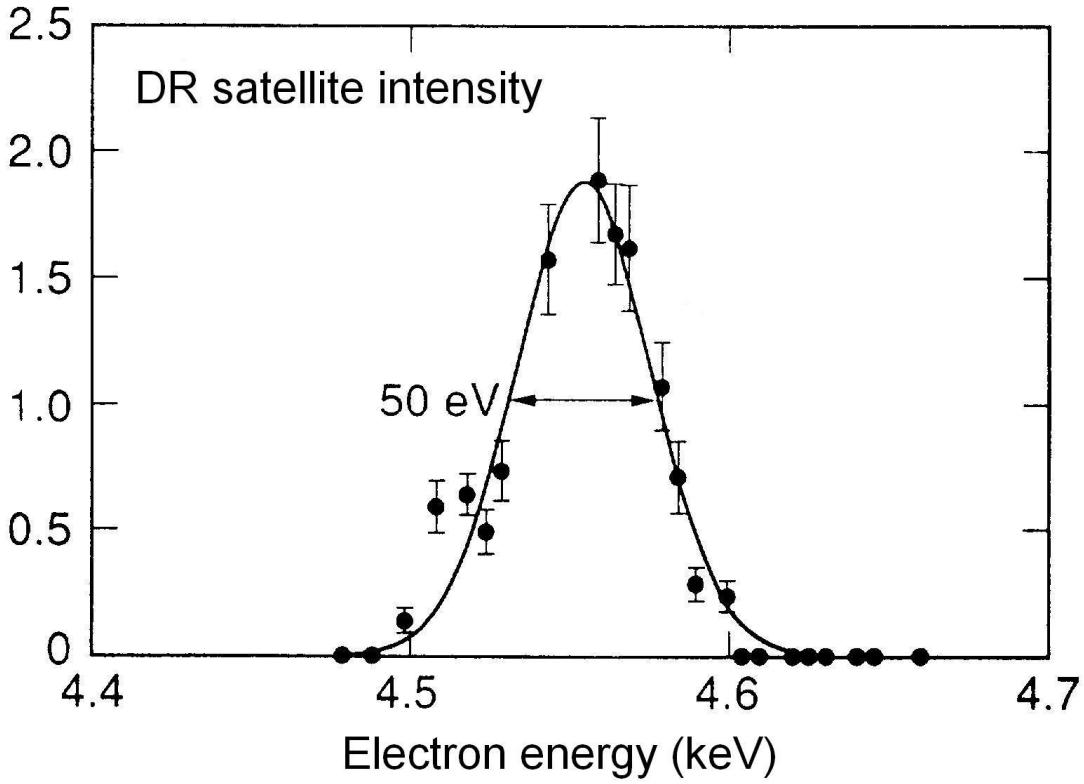
DR satellite intensity
50 eV
2.5
2.0
1.5
1.0
0.5
0
4.4
4.5
4.6
4.7
Electron energy (keV)

Figure 4

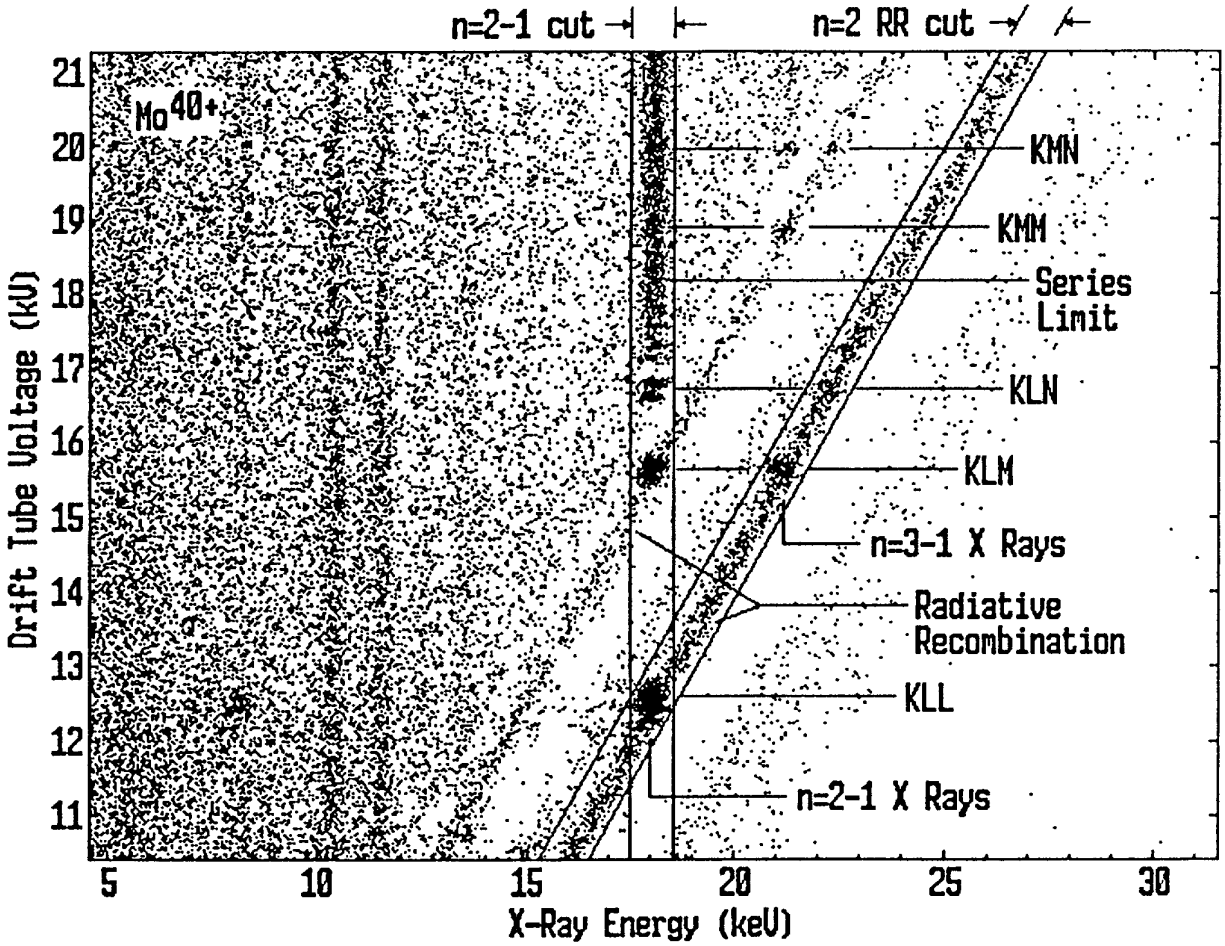
n=2-1 cut
n=2 RR cut
Mo40+
KMN
KMM
Series Limit
KLN
KLM
n=3-1 X Rays
Radiative Recombination
KLL
n=2-1 X Rays
Drift Tube Voltage (kV)
X-Ray Energy (keV)
21
20
19
18
17
16
15
14
13
12
11
5
10
15
20
25
30

Figure 5

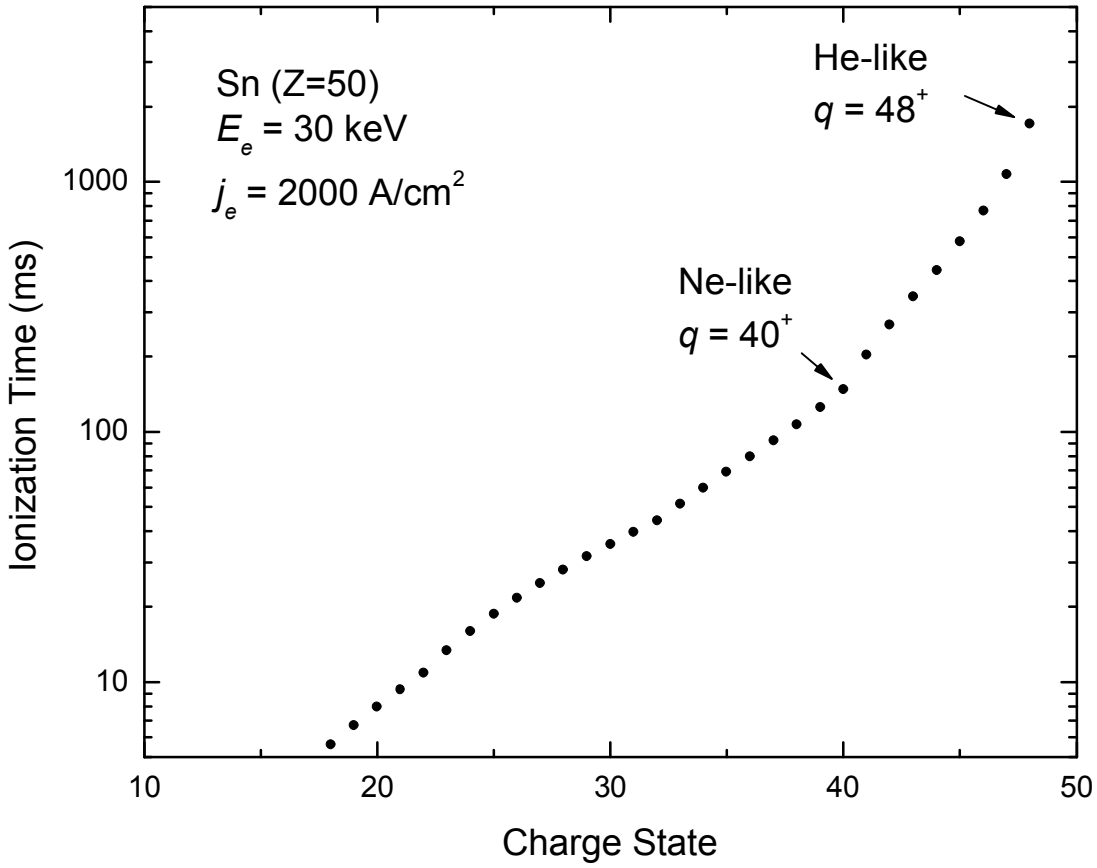
Sn (Z=50)
E_e = 30 keV
j_e = 2000 A/cm^2
He-like
q = 48$^+$
Ne-like
q = 40$^+$
Ionization Time (ms)
1000
100
10
10
20
30
40
50
Charge State

Figure 6

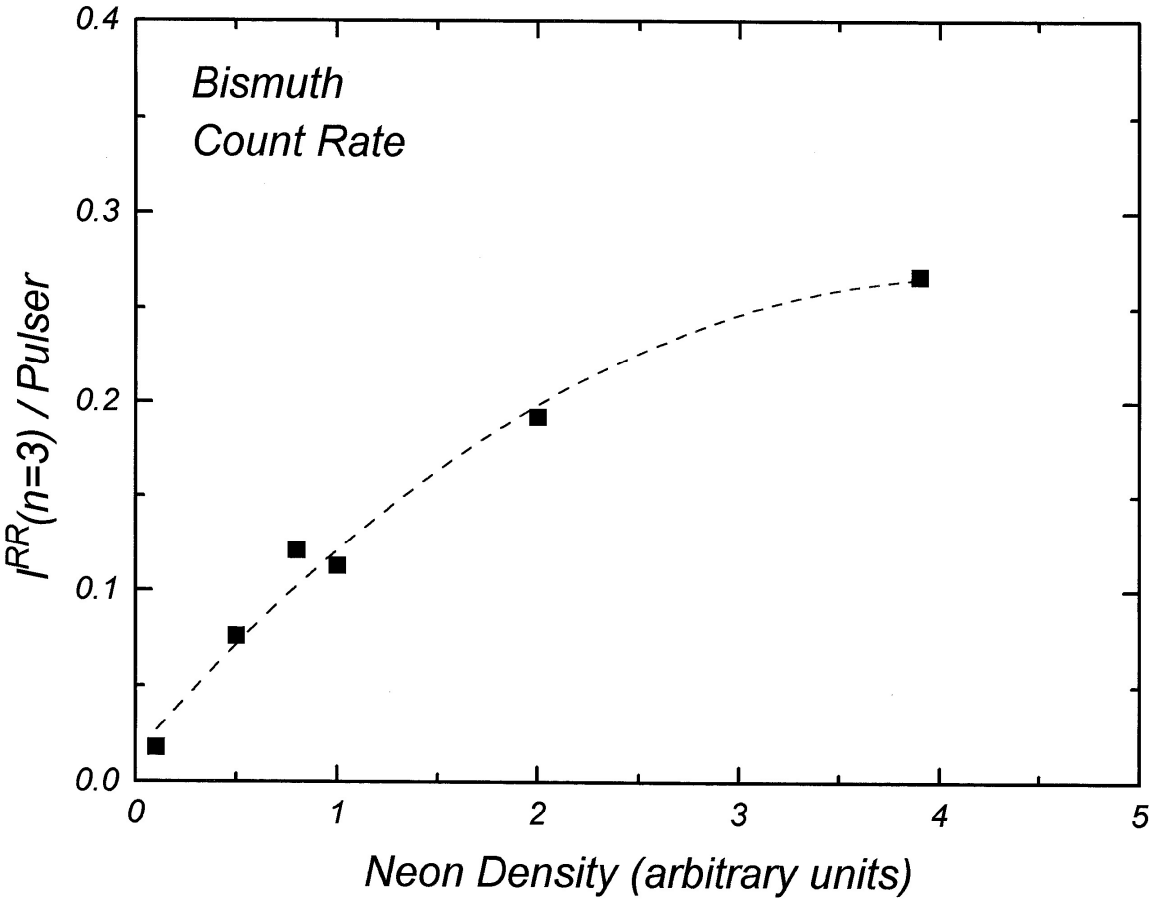
Bismuth
Count Rate
$I^{RR}(n=3)$ / Pulser
0.0
0.1
0.2
0.3
0.4
0
1
2
3
4
5
Neon Density (arbitrary units)

Figure 7

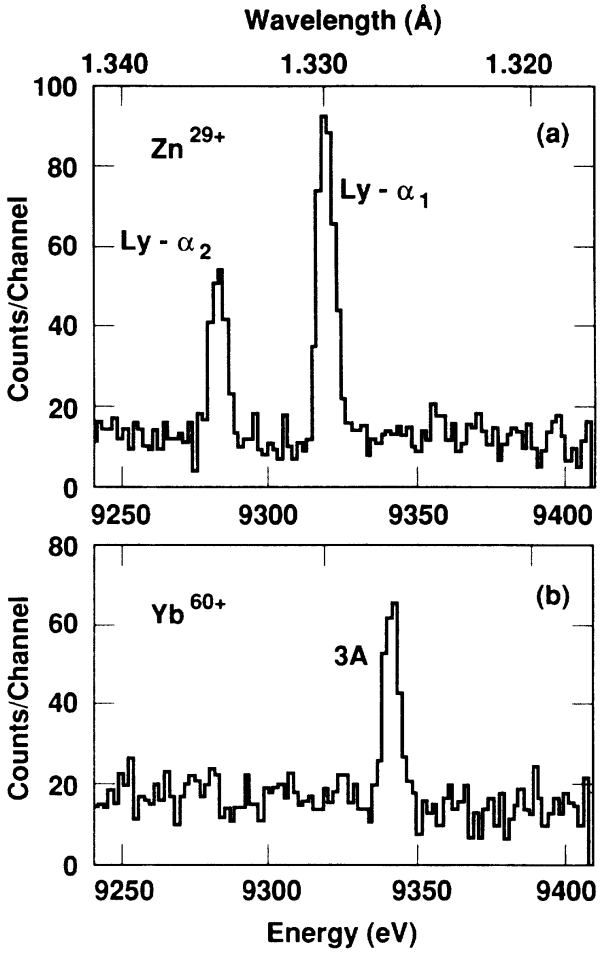
Wavelength (Å)
1.340
1.330
1.320
Zn 29+
(a)
Ly - α1
Ly - α2
Counts/Channel
Yb 60+
(b)
3A
Energy (eV)

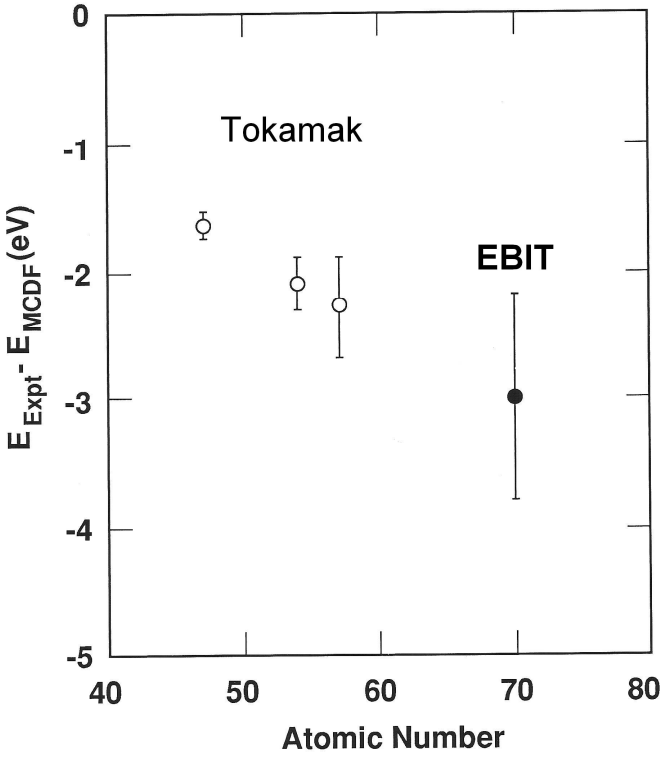
Tokamak
EBIT
E Expt - E MCDF (eV)
Atomic Number

Figure 8

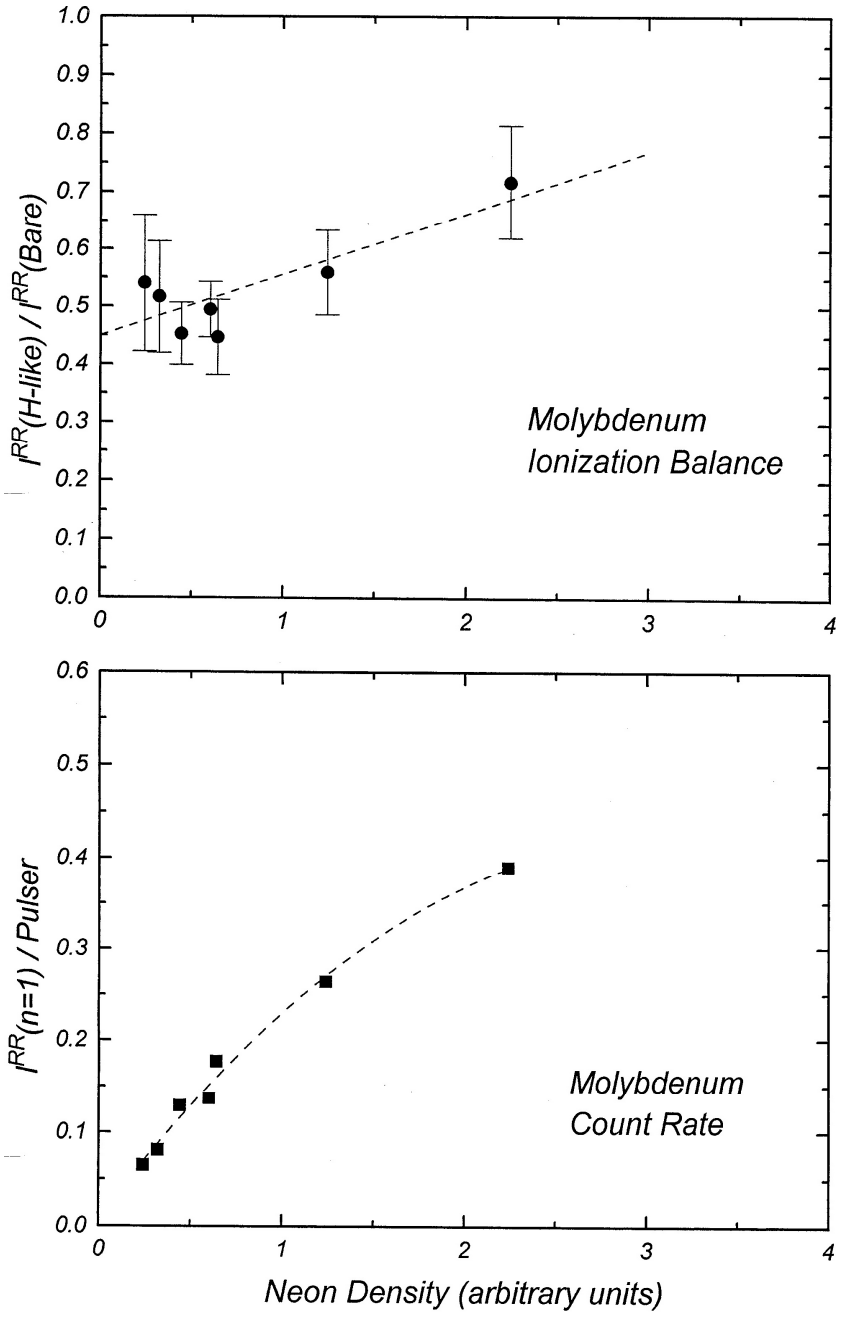
1.0
0.9
0.8
0.7
0.6
0.5
0.4
0.3
0.2
0.1
0.0
0
1
2
3
4
I^{RR}(H-like) / I^{RR}(Bare)
Molybdenum
Ionization Balance
0.6
0.5
0.4
0.3
0.2
0.1
0.0
I^{RR}(n=1) / Pulser
Molybdenum
Count Rate
Neon Density (arbitrary units)

Figure 9

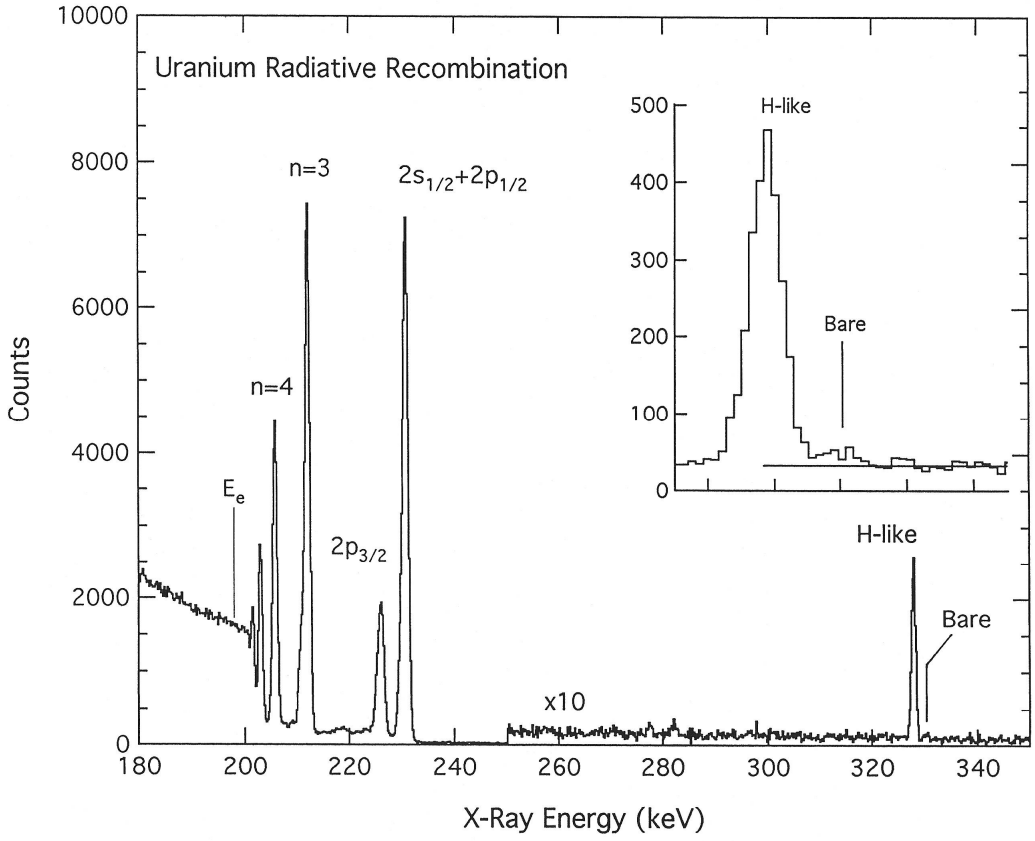
Uranium Radiative Recombination
Counts
X-Ray Energy (keV)
10000
8000
6000
4000
2000
0
180
200
220
240
260
280
300
320
340
n=3
$2s_{1/2}+2p_{1/2}$
n=4
E_e
$2p_{3/2}$
x10
H-like
Bare
500
400
300
200
100
0
H-like
Bare

Figure 10

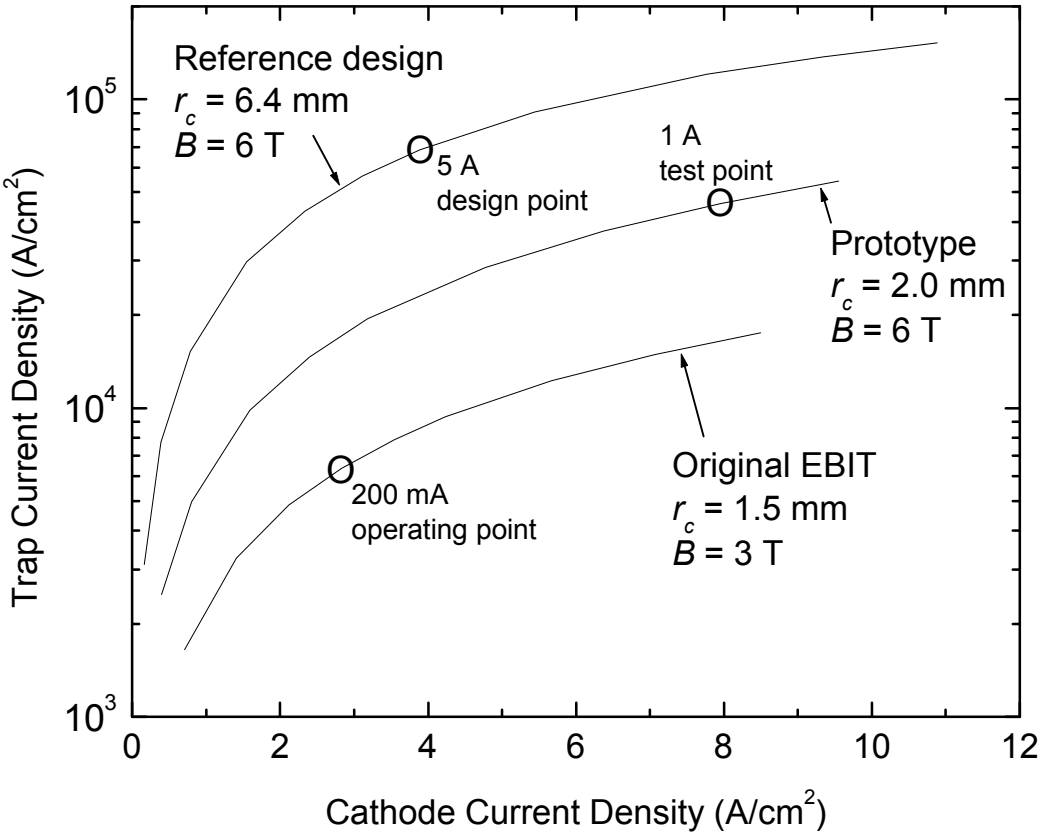
Reference design
r_c = 6.4 mm
B = 6 T
5 A
design point
1 A
test point
Prototype
r_c = 2.0 mm
B = 6 T
200 mA
operating point
Original EBIT
r_c = 1.5 mm
B = 3 T
10^5
10^4
10^3
0
2
4
6
8
10
12
Trap Current Density (A/cm^2)
Cathode Current Density (A/cm^2)

Figure 11